Radiological Physics and Technology (2019) 12:260–267
https://doi.org/10.1007/s12194-019-00516-8

A complementary scheme for automated detection of high-uptake regions on dedicated breast PET and whole-body PET/CT

Natsuki Minoura[1,2] · Atsushi Teramoto[1] · Akari Ito[3] · Osamu Yamamuro[3] · Masami Nishio[4] · Kuniaki Saito[1] · Hiroshi Fujita[5]

Received: 10 January 2019 / Revised: 16 May 2019 / Accepted: 17 May 2019 / Published online: 25 May 2019

Abstract
In this study, we aimed to develop a hybrid method for automated detection of high-uptake regions in the breast and axilla using dedicated breast positron-emission tomography (db PET) and whole-body PET/computed tomography (CT) images. In our proposed method, high-uptake regions in the breast and axilla were detected using db PET images and whole-body PET/CT images. In db PET images, high-uptake regions in the breast were detected using adaptive thresholding technique based on the noise characteristics. In whole-body PET/CT images, the region of the breast that includes the axilla was first extracted using CT images. Next, high-uptake regions in the extracted breast region were detected on the PET images. By integration of the results of the two types of PET images, a final candidate region was obtained. In the experiments, the accuracy of extracting the region of the breast and detection ability was evaluated using clinical data. As a result, all breast regions were extracted correctly. The sensitivity of detection was 0.765, and the number of false positive cases were 1.8, which was 30% better than those on whole-body PET/CT alone. These results suggested that the proposed method, combining the two types of PET images is effective for improving detection performance.

Keywords Dedicated breast pet · Whole-body PET/CT · Image processing · Breast cancer

1 Introduction

Breast cancer is the leading cause of cancer-related deaths among women [1]. Imaging modalities for the diagnosis of breast cancer include mammography, breast ultrasound, breast magnetic resonance imaging (MRI) and positron emission tomography (PET). Mammography and breast ultrasound provide anatomical information, while breast MRI and PET provide functional information. In particular, ^{18}F-fluorodeoxyglucose (FDG) PET provides functional information, which is reflected in glucose metabolism and tissue uptake.

In breast cancer, PET is mainly used for staging or assessment of treatment response. Since many PET systems are hybrid modalities of computed tomography (CT), whole-body anatomical information from CT images and functional information from PET images can be obtained together. The two types of information can help radiologists to arrive at a diagnosis. However, detection of early breast tumors with diameter less than 1 cm using whole-body PET/CT images is challenging owing to limited spatial resolution of whole-body PET detectors [2].

In recent years, dedicated breast PET (db PET) has been developed, which is a PET scanner for breasts with high spatial resolution [2]. This technique includes the opposite-type and the ring-type db PET scanners. In the former, the breast is compressed by two planar detectors and a tomographic image can be obtained parallel to the detectors. In the latter, the breast is scanned by dropping it to the center of the O type or C type detector [3].

✉ Atsushi Teramoto
teramoto@fujita-hu.ac.jp

1 Graduate School of Health Sciences, Fujita Health University, 1-98 Dengakugakubo, Kutsukake, Toyoake, Aichi 470-1192, Japan

2 Nagoya City University Hospital, Nagoya, Japan

3 East Nagoya Imaging Diagnosis Center, Nagoya, Japan

4 Nagoya PET Imaging Center, Nagoya, Japan

5 Department of Electrical, Electronic and Computer Engineering, Faculty of Engineering, Gifu University, Gifu, Japan

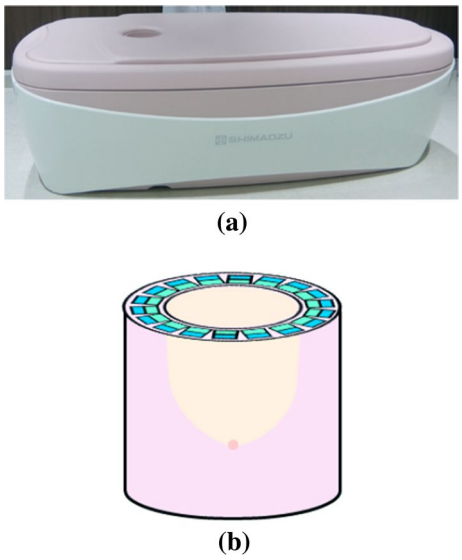

Fig. 1 Ring-type dedicated breast PET scanner. **a** The appearance of the scanner and **b** detectors of the scanner

Figure 1a shows the appearance of a ring-type db PET scanner. The left and right breasts are placed in the detector one at a time, and volume data are obtained. The crystal element of the db PET scanner is very small and has high resolution; thereby enabling detection of lesions with a diameter of less than 1 cm [4].

Recently, several studies have reported on the advantages of db PET. Reports on the evaluation of performance [4, 5] suggest that db PET has high spatial resolution and is useful for the detection of small breast lesions. Furthermore, recent studies have also reported on the diagnostic performance of db PET compared with that of whole-body PET/CT [6–8]. However, there are currently few reports on image processing technology using db PET images.

Computer-aided diagnosis (CAD) is one of the medical image processing techniques used in the diagnosis of breast cancer. CAD provides a computerized output as a "second opinion" to support the diagnosis by the radiologist [9–11]. CAD techniques such as methods for detecting masses, micro-calcifications, and architectural distortion have been developed for breast cancer using mammograms [12–16]. Additionally, methods for detection of masses using breast ultrasound images [17, 18], automated analysis of breast density and differentiation between benign and malignant lesions using breast MR images have been proposed [19, 20]. Furthermore, automated detection methods of breast tumors and axillary metastases using PET and CT images obtained from whole-body PET/CT have been proposed [21]. Using this detection method [21], breast tumors, which increased highly or had large diameters were detected. However, due to the limitations of the spatial resolution of whole-body PET images, lesions with diameters less than 1 cm are not clearly detected. In addition, there are no reports on CAD technology for db PET images.

In this study, we propose a new technique to support the automated detection of breast cancer, we set out to add automated detection processing of small high-uptake regions, using db PET images, to the previously established automated detection processing [21]. As a preliminary study, a method for automated detection of high-uptake regions in the breast and axilla was developed by combining two types of PET images complementarily.

2 Materials and methods

2.1 Clinical data

The Institutional Review Board of East Nagoya Imaging Diagnosis Center (RE160101) approved the present study. All images were anonymized prior to use.

To evaluate the detection ability of the scheme in the present study, 24 cases with db PET images and whole-body PET/CT images were collected. The data set included 12 abnormal scans with high-uptake regions in the breast and axilla and 12 normal scans. The images were acquired at the East Nagoya Imaging Diagnosis Center (Nagoya, Japan) using an Elmammo db PET scanner (Shimadzu, Kyoto, Japan) and True Point Biograph 40 PET/CT scanner (Siemens, Munich, Germany). Both PET scans were performed on the same day. The patients underwent a whole-body PET/CT scan at 90 min after an injection of FDG 196 ± 31.2 MBq, followed by a db PET scan of the right and left breasts approximately 110 min after the injection. The acquisition time of a db PET scan was 7 (13 cases) or 10 min (11 cases) and that of a whole-body PET scan was 11.88 ± 1.72 min. Since the imaging protocol was changed in the data collection period, the clinical data included two types of acquisition time. The volume data of db PET were reconstructed directly with a three-dimensional dynamic row-action maximum-likelihood algorithm [22] using 128 subsets, 1 iteration, and relaxation control parameter $\beta = 20$.

The db PET images were attenuation-corrected using a uniform attenuation map with object boundaries obtained from the emission data [4] and scatter-corrected. The size of the matrices was 236×200 pixels, and the voxel size was $0.78 \times 0.78 \times 0.78$ mm^3. Acquisition conditions of whole-body CT images were as follows: the size of the matrices was 512×512 pixels, and the voxel size was $0.97 \times 0.97 \times 2.00$ mm^3. The tube voltage was 120 kV, and the slice thickness was set at 2.0 mm. B19f was used in the reconstruction function. Whole-body PET images were attenuation-corrected using CT data and were scatter-corrected. The images were reconstructed with an ordered-subsets expectation–maximization algorithm called

High-Definition PET Reconstruction (21 subsets, 3 iterations). The size of the matrices was 168 × 168 pixels, and the voxel size was 4.0 × 4.0 × 2.0 mm^3. Fifty-one high-uptake regions (breast: 36, axilla: 15) were detected by a board-certified PET nuclear medicine radiologist (Japanese Society of Nuclear Medicine, in Japanese) with 18 years of experience in PET. Among them, 19 high-uptake regions in the breast were detected only in db PET images and had diameters of approximately 3–5 mm. The average diameter of the high-uptake regions included in the 24 cases was 13.7 ± 9.46 mm; the average value of the standardized uptake value (SUV) max was 4.09 ± 3.60 in the whole-body PET/CT images, and 7.58 ± 6.74 in db PET images.

2.2 Overview of automated detection method

Figure 2 shows a flowchart of automated detection processing of high-uptake regions in the breast and axilla using db PET images and whole-body PET/CT images. In the method proposed in the present study, high-uptake regions in the breast and axilla are detected using three types of images: db PET images, whole-body PET images, and whole-body CT images. In db PET images, high-uptake regions in the breast are detected. In whole-body PET/CT images, a breast region that includes the axilla is extracted using CT images, and high-uptake regions in the breast region are detected from PET images. By integrating the detection results of the two types of PET images, a final candidate region can be obtained. The procedure has been described below.

2.3 Automated detection of small high-uptake regions in breast using dedicated breast PET images

2.3.1 SUV transformation

Tissue radioactivity levels can be obtained from PET images; however, the measurement varies with the injected dose and weight of the patient. Therefore, the SUV is calculated for each image as the ratio of the measured activity to the injected dose/body weight [23]:

$$\mathrm{SUV} = \frac{\text{Measured activity (Bq/kg)}}{\text{Injected dose (Bq)/body weight (kg)}}. \quad (1)$$

2.3.2 Thresholding

Figure 3 shows the relationship between the slice position of the db PET scanner and the standard deviation of noise. As shown in Fig. 3, the db PET image has high noise level at the edge of the detector (the bottom of the detector or the chest wall side); however, it may contain important information. Additionally, when all of the slice images are binarized with the same cut-off value, more noise is detected at the edge of the detector and false positives increase. In the proposed method, the cut-off value was selectively changed, based on the noise characteristics of each slice.

Figure 4b shows the relationship between the slice position i of the db PET image and the standard deviation of noise Sd_i. Subsequently, the relationship between Sd_i and Th_{di} was obtained in advance to prevent noise detection using a normal case, and the a and b in formula (2) were calculated (Fig. 4c).

$$\mathrm{Th}_{di} = a \times Sd_i + b. \quad (2)$$

By substituting Sd_i into Eq. (2), the relationship between i and Th_{di} was obtained (Fig. 4d). As shown in Fig. 4d, Th_{di} was selectively set to be low for the slice near the center and high for the peripheral aspect. The db PET image (Fig. 4a) was binarized using the determined cut-off values (Fig. 4e).

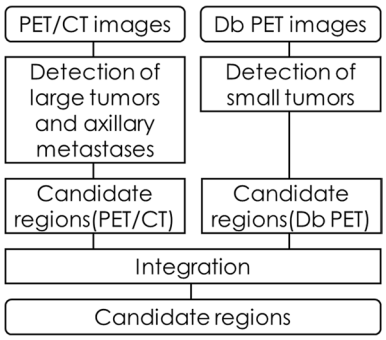

Fig. 2 Overview of the proposed method

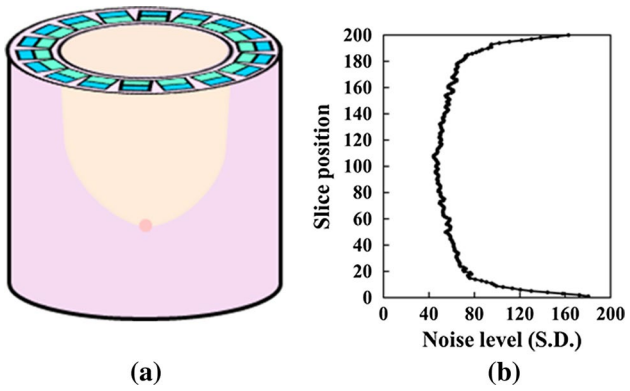

Fig. 3 Noise characteristics of the dedicated breast PET (db PET) scanner. **a** db PET and **b** Graph showing the relationship between slice position and noise level (S.D.)

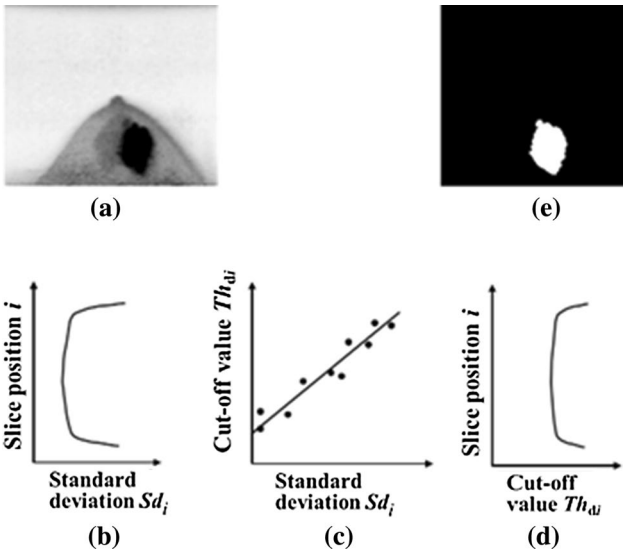

Fig. 4 Detection of high-uptake regions in the breast in the dedicated breast PET (db PET) images. **a** Original dbPET image, **b** noise characteristics, **c** relationship between Th_{di} and Sd_i, **d** Cut-off values and **e** binarized image

2.3.3 Labeling

By applying the labeling to the binarized image, the high-uptake regions can be detected and candidate regions in the breast obtained.

2.4 Automated detection of high-uptake regions in the breast and axilla using whole-body PET/CT images

High-uptake regions in the breast and axilla were detected by the main procedure shown in Fig. 5 and already described elsewhere [21]. The procedure involved the extraction of a region of the breast including the axilla from the CT images, following which high-uptake regions were detected from the PET images.

In CT images, the region of the breast that includes the axilla was defined using the anatomical information of the lungs and scapula. The defined breast region was acquired

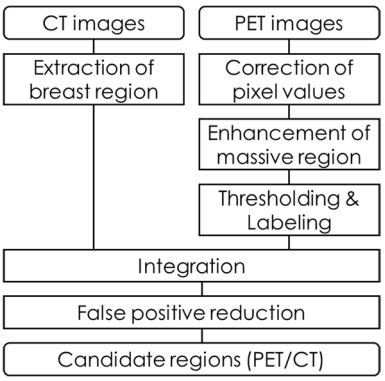

Fig. 5 Flowchart of the detection method in whole-body PET/CT images

using the bone and lung region of CT images obtained by binarization or morphological processing (Fig. 6a).

In PET images (Fig. 6b), the SUV was first calculated for each pixel value. Second, to detect slightly high-uptake regions, the ball-like regions were enhanced using the eigenvalues of the Hessian matrix [24]. Thereafter, a high-uptake region inside the region of the breast obtained from CT images was detected using the cut-off value of Th_p, which is used for detecting the initial candidate region (Fig. 6c).

2.5 Integration

Candidate regions detected by db PET and whole-body PET/CT were represented as binary images. After visual inspection of the presence of the regions in both images, the region detected by at least one modality was treated as the candidate region. Using the above processing, the final candidate regions were obtained.

2.6 Evaluation methods

In the experiments, the accuracy of extracting the region of the breast and the detection ability of high-uptake regions were evaluated. A region of the breast was considered to be extracted correctly if it contained a sufficient portion of the axilla on visual inspection. The candidate region was judged as true positive if the center of the coordinates of

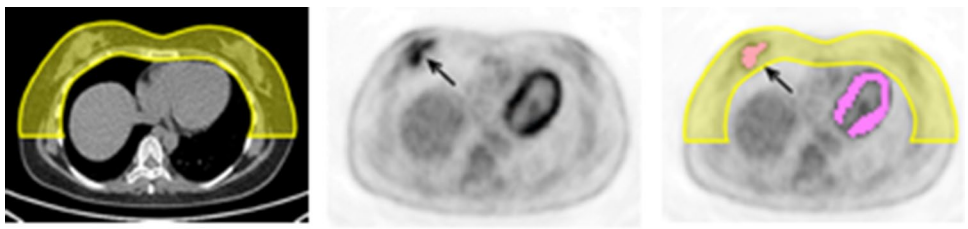

Fig. 6 Detection of high-uptake regions in the breast and axilla in whole-body PET/CT images. **a** CT image (breast region), **b** original PET image, **c** detected image (the yellow regions indicate the region of the breast and the arrows indicate the detected high-uptake regions in the breast)

the high-uptake regions, as indicated by the radiologist, was present within the range of a predetermined distance from the candidate region.

The detection parameters were as follows: Th_{bone} was 150 [H.U.] and Th_{breast} was −500 [H.U.]. For Th_{di}, the results of a preliminary examination from a normal case were used. To reduce the incidence of false positives, candidate regions with volume < 19 pixels ($V_{FP} = 19$) were judged as false positives. To emphasize the small and low-uptake lesions, the enhancement parameters were set as $\sigma_H = 1.5$, $M_1 = 10^7$, $M_2 = 1.5 \times 10^7$, $E_1 = 1.0$, $E_2 = 1.5$ [21]. These parameters were defined in a previous report. We developed a CAD software using Visual Studio 2012 (Microsoft).

During the current evaluation, true positive rate (TPR) and the number of false positives per case (FPs/case) were calculated by changing the detection thresholds, Th_{di} and Th_p. Here, TPR was defined as the ratio of the number of high-uptake regions detected to the number of high-uptake regions identified by a radiologist and was expressed as a percentage. The FPs/case was calculated using normal cases. Furthermore, free-response receiver operating characteristic (FROC) curves for whole-body PET/CT detection alone were obtained to allow comparison with the hybrid detection approach.

3 Results

All regions were extracted correctly. Figure 7a presents the FROC curves for whole-body PET/CT detection and hybrid detection (db PET + whole-body PET/CT). In the hybrid detection method, the sensitivity of detection was 0.765, with a FP/case of 1.8. By combining db PET images and whole-body PET/CT images, the sensitivity of detection was approximately 30% higher than that of whole-body PET/CT images alone. To analyze these results in detail, FROC curves of detection were used based on whole-body PET/CT images and db PET images for high-uptake regions in the breast and axilla, respectively (Fig. 7b, c). Additionally, approximately 86% of high-uptake regions in the breast were detected using whole-body PET/CT images and db PET images in as shown in Fig. 7b. The hybrid detection method used in the present study was approximately 46% more accurate than the conventional method based on whole-body PET/CT images alone. In addition, approximately 60% of high-uptake regions in the axilla were detected using the whole-body PET/CT images (Fig. 7c). The detection results are shown in Figs. 8, 9 and 10.

Figures 8 and 9 show examples of the high-uptake regions detected inside the region of the breast. A case of right breast cancer (N0M0) is shown in Fig. 8. The high-uptake regions identified by a radiologist in the right breast are indicated in Fig. 8. Figure 8b, c shows the same high-uptake region as

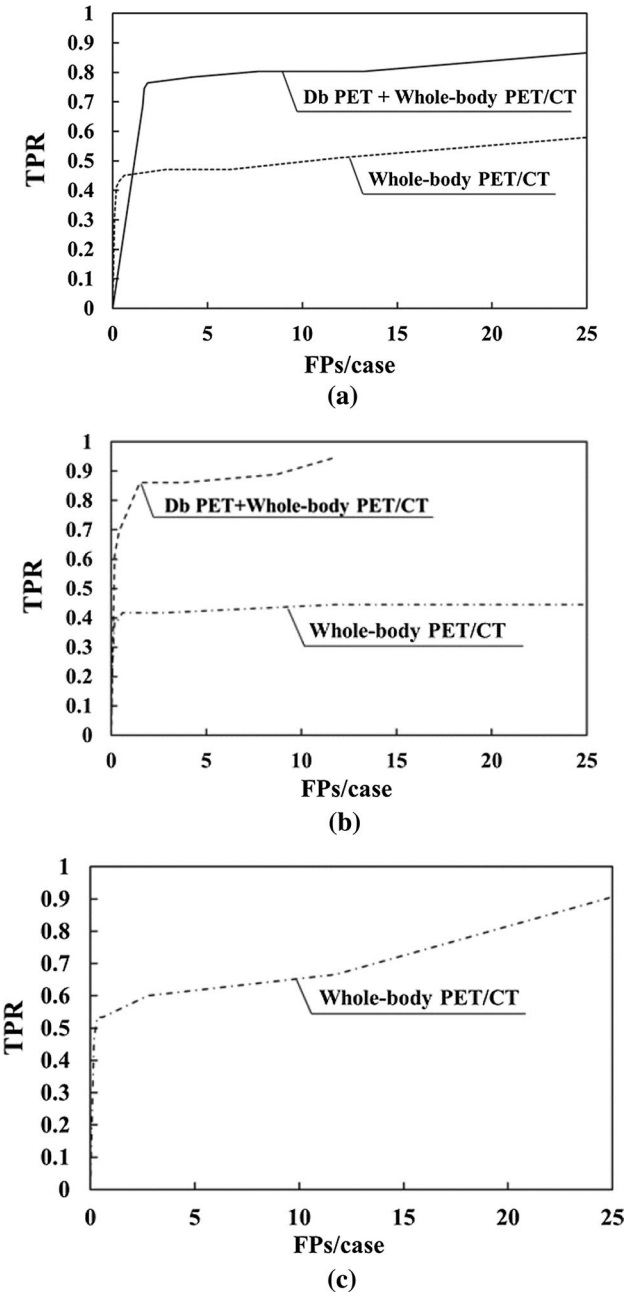

Fig. 7 Free-response receiver operating characteristic (FROC) curves showing the relationship between TPR and FPs/case while changing Th_{di} and Th_p

detected by the whole-body PET/CT image and the right db PET images, respectively. In addition, a small high-uptake region in the breast with a diameter of approximately 4 mm was detected in the left db PET image (Fig. 8d). This region was detected by db PET images alone.

In Fig. 9, a case of right breast cancer (N1M0) is shown. The high-uptake regions identified by a radiologist in the right axilla and the right breast are indicated in Fig. 9a. As shown in Fig. 9b, the same high-uptake region in the axilla

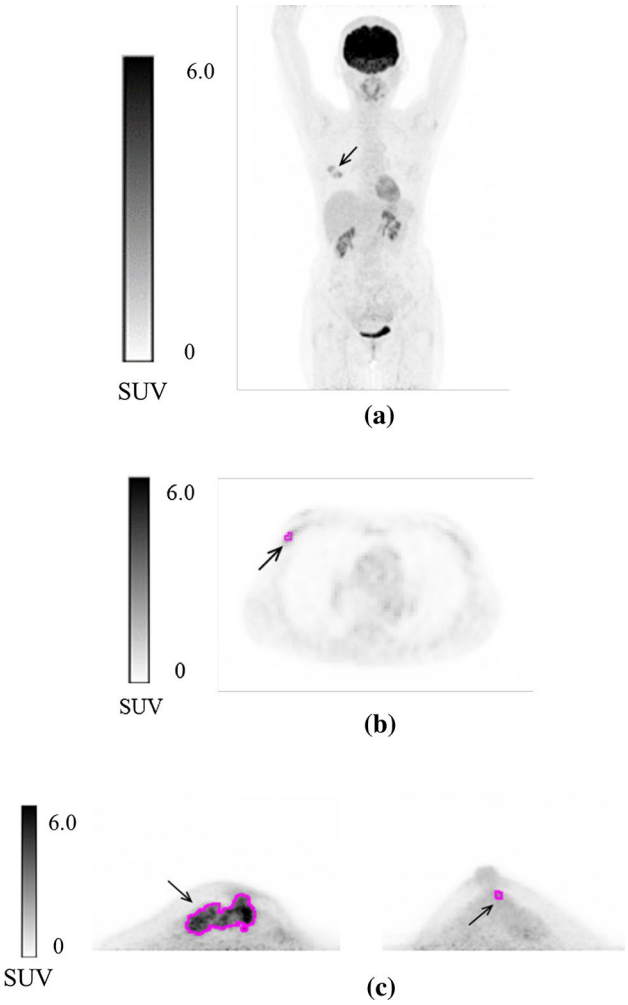

Fig. 8 Detection example 1. The pink areas indicate the detected regions. **a** Whole-body PET image (maximum intensity projection, MIP), **b** whole-body PET image (axial), **c** dedicated breast PET image (MIP) of the right breast and **d** dedicated breast PET image (MIP) of the left breast

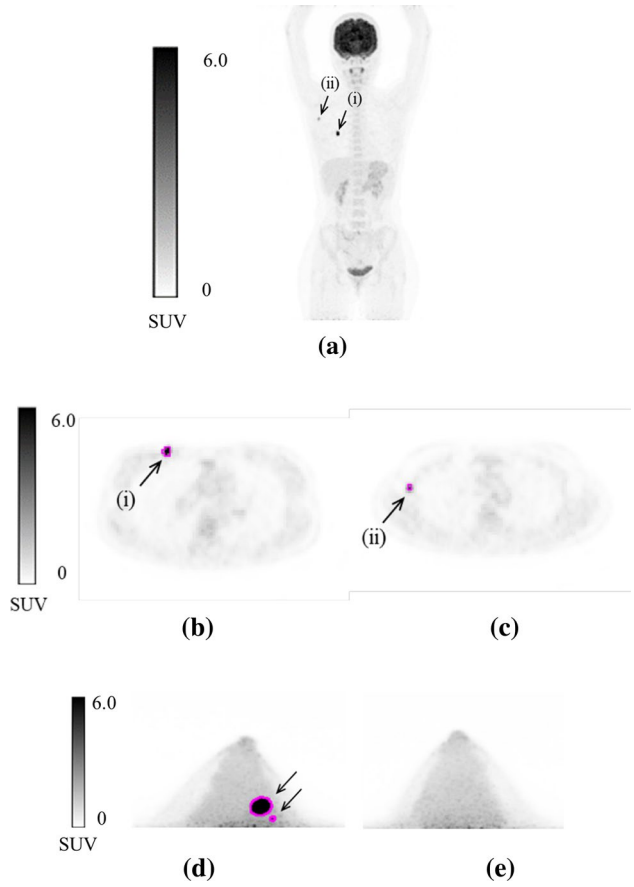

Fig. 9 Detection example 2. The pink areas indicated the detected regions. As in Fig. 8, **a** is the whole-body PET image (MIP). **b** and **c** are the whole-body PET images (axial) at the position of (i) and (ii), respectively. **d** and **e** are the right and left db PET images (MIP), respectively

was detected in the whole-body PET/CT image. Additionally, Fig. 9c, d shows the same high-uptake region in the breast as detected in the whole-body PET/CT image and the right db PET image, respectively. In addition, Fig. 9d indicates a small high-uptake region in the breast with a diameter of about 4 mm on the chest wall side. This region was detected by db PET images alone.

Additionally, Fig. 10 shows an example of db PET images of high-uptake regions in the breast that were not detected. These are small high-uptake regions in the breast with diameters of 3-5 mm that were not detected in whole-body PET/CT images (arrows).

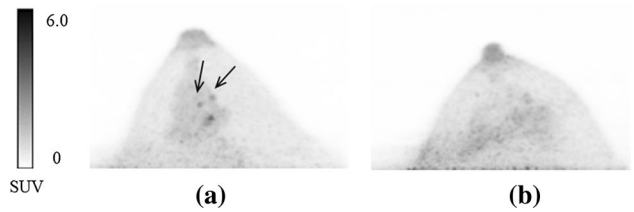

Fig. 10 Undetected example. Dedicated breast PET image (MIP) of the left breast. Arrows indicate undetected high-uptake regions

4 Discussion

The current study added further automated processing for the detection of small high-uptake regions in the breast in db PET images. The study also pioneered an approach for automated detection of high-uptake regions in the breast and axilla by combining two types of PET images.

As shown in Fig. 7a, the sensitivity of detection using the two types of PET images was 30% higher than that achieved using whole-body PET/CT images alone.

The high-uptake regions in the breast detected in Fig. 8b, c measured approximately 20 mm in diameter (whole-body PET) and had a SUV_{max} of 2.54 (whole-body PET), representing a large diameter and high-uptake [25]. The high-uptake regions in the breast detected in Fig. 8d was a small region with a diameter of approximately 4 mm (db PET); however, the SUV was higher than that of the mammary gland and nipple, thereby resulting in detection. Next, the high-uptake region in the axilla detected in Fig. 9b measured approximately 8 mm in diameter (whole-body PET) and had a SUV_{max} of 4.68 (whole-body PET). Since the high-uptake regions in the axilla were outside the field of view in db PET images, detection was possible only from the whole-body PET/CT images. The high-uptake region in the breast detected in Fig. 9e was approximately 4 mm in diameter (db PET) and was located near the chest wall with high noise level; however, was detected due to high SUV_{max} (6.15) (db PET). Thus, in the proposed method, small high-uptake regions in the breast were detected using db PET images, whereas all high-uptake regions in the axilla were detected using whole-body PET/CT images by the radiologist. These results suggest that the hybrid detection method proposed in the present study, combining the two types of PET images, is useful. It may be possible to reduce the burden of interpretation when detecting abnormal cases from a large number of normal cases, such as during screening. Alternatively, many PET images can be input in the CAD system, which could avoid misdiagnosis and improve sensitivity.

In a previous report, the detection ability was 76% with 3.9 FPs/case [21]. The detection performance noted in this study using the proposed method did not change significantly from that noted in the previous study, which used the conventional method. The clinical data used in this paper were different from those used in the previous paper [21]. However, the algorithms and parameters used for automated detection of high-uptake regions in the breast and axilla using whole-body PET/CT images were the same as in the previous study, which used the conventional method [21]. Based on these aspects, it was speculated that the clinical data used in this paper contained many high-uptake regions that were difficult to detect.

The high-uptake region in the breast shown in Fig. 10 demonstrated low-uptake among other similar regions identified from db PET images ($SUV_{max} = 2.22$) by the radiologist. In addition, the slice position where the region exists was close to the edge of the detector, and the cut-off value determined considering the standard deviation of the noise was 2.65. In the proposed method, cut-off values were set in advance to avoid detection of noise when using a normal case; therefore, detection of the high-uptake region in the breast was difficult, as shown in Fig. 10. Future studies must consider improved threshold-setting methods for the detection of small high-uptake regions in the breast. In addition, we need to investigate the detection performance by changing several factors affecting the image quality, such as imaging time and fasting time.

5 Study limitations

The major limitation of the present study is the number of cases used in the proposed method. A larger sample size is required to evaluate the detection performance. Furthermore, the detection results should be evaluated using data of high-uptake regions identified by multiple radiologists and compared with the pathological results. As it was a preliminary study, high-uptake regions were determined by a radiologist who was familiar with PET-based diagnosis. In the future, we would evaluate the detection performance using high-uptake regions identified by multiple radiologists for a more detailed evaluation.

6 Conclusion

The present study developed a hybrid method for the detection of high-uptake regions in the breast and axilla using dedicated breast PET images and whole-body PET/CT images. Experimental results indicate that the proposed method, combining two types of PET images, is effective for improving detection performance in the breast region.

Funding The present research was supported in part by a Grant-in-Aid for Scientific Research on Innovative Areas (#26108005), MEXT, Japan.

Compliance with ethical standards

Ethical approval All procedures in studies involving human participants were performed in accordance with the ethical standards of the institutional and/or national research committee and with the 1964 Helsinki Declaration and its later amendments or comparable ethical standards.

Research involving human participants and animals The present article does not contain any studies done on animals performed by any of the authors.

Informed consent Patient agreements were obtained given the condition that all data were anonymized.

References

1. Breast cancer: facts and figures 2017–2018. American Cancer Society. 2017. https://www.cancer.org/content/dam/cancer-org/research/cancer-facts-and-statistics/breast-cancer-facts-and-figures/breast-cancer-facts-and-figures-2017-2018.pdf. Accessed 21 Jan 2019.
2. Vercher-Conejero JL, Pelegrí-Martinez L, Lopez-Aznar D, Cózar-Santiago Mdel P. Positron emission tomography in breast cancer. Diagnostics (Basel). 2015;5:61–83.
3. Hosono M, Saga T, Ito K, Kumita S, Sasaki M, Senda M, Hatazawa J, Watanabe H, Ito H, Kanaya S, Kimura Y, Saji H, Jinnouchi S, Fukukita H, Murakami K, Kinuya S, Yamazaki J, Uchiyama M, Uno K, Kato K, Kawano T, Kubota K, Togawa T, Honda N, Maruno H, Yoshimura M, Kawamoto M, Ozawa Y. Clinical practice guideline for dedicated breast PET. Ann Nucl Med. 2014;28:597–602.
4. Miyake KK, Matsumoto K, Inoue M, Nakamoto Y, Kanao S, Oishi T, Kawase S, Kitamura K, Yamakawa Y, Akazawa A, Kobayashi T, Ohi J, Togashi K. Performance evaluation of a new dedicated breast PET scanner using NEMA NU4-2008 standards. J Nucl Med. 2014;55:1198–203.
5. García Hernández T, Vicedo González A, Ferrer Rebolleda J, Sánchez Jurado R, Roselló Ferrando J, Brualla González L, Granero Cabañero D, Del Puig Cozar Santiago M. Performance evaluation of a high resolution dedicated breast PET scanner. Med Phys. 2016;43:2261–72.
6. Teixeira SC, Rebolleda JF, Koolen BB, Wesseling J, Jurado RS, Stokkel MP, Del Puig Cózar Santiago M, van der Noort V, Rutgers EJ, Valdés Olmos RA. Evaluation of a hanging-breast PET system for primary tumor visualization in patients with stage I-III breast cancer: comparison with standard PET/CT. Am J Roentgenol. 2016;206:1307–14.
7. Iima M, Nakamoto Y, Kanao S, Sugie T, Ueno T, Kawada M, Mikami Y, Toi M, Togashi K. Clinical performance of 2 dedicated PET scanners for breast imaging: initial evaluation. J Nucl Med. 2012;53:1534–42.
8. Nishimatsu K, Nakamoto Y, Miyake KK, Ishimori T, Kanao S, Toi M, et al. Higher breast cancer conspicuity on db PET compared to WB-PET/CT. Eur J Radiol. 2017;90:138–45.
9. Fujita H, Uchiyama Y, Nakagawa T, Fukuoka D, Hatanaka Y, Hara T, Lee GN, Hayashi Y, Ikedo Y, Gao X, Zhou X. Computer-aided diagnosis: the emerging of three CAD systems induced by Japanese health care needs. Comput Methods Programs Biomed. 2008;92:238–48.
10. Teramoto A, Fujita H, Takahashi K, Yamamuro O, Tamaki T, Nishio M, Kobayashi T. Hybrid method for the detection of pulmonary nodules using positron emission tomography/computed tomography: a preliminary study. Int J Comput Assist Radiol Surg. 2014;9:59–69.
11. Teramoto A, Fujita H, Yamamuro O, Tamaki T. Automated detection of pulmonary nodules in PET/CT images: ensemble false-positive reduction using a convolutional neural network technique. Med Phys. 2016;43:2821–7.
12. Cheng HD, Shi XJ, Min R, Hu LM, Cai XP, Du HN. Approaches for automated detection and classification of masses in mammograms. Pattern Recognit. 2006;39:646–68.
13. Yu S, Guan L. A CAD system for the automatic detection of clustered microcalcifications in digitized mammogram films. IEEE Trans Med Imaging. 2000;19:115–26.
14. Dong M, Lu X, Ma Y, Guo Y, Ma Y, Wang K. An efficient approach for automated mass segmentation and classification in mammograms. J Digit Imaging. 2015;28:613–25.
15. Rangayyan RM, Banik S, Chakraborty J, Mukhopadhyay S, Desautels JE. Measure of divergence of oriented patterns for the detection of architectural distortion in prior mammograms. Int J Comput Assist Radiol Surg. 2013;8:527–45.
16. Yoshikawa R, Teramoto A, Matsubara T, Fujita H. Automated detection of architectural distortion using improved adaptive Gabor filter. In: Proceedings of IWDM. 2014. pp. 606–11.
17. Ikedo Y, Fukuoka D, Hara T, Fujita H, Takada E, Endo T, Morita T. Development of a fully automatic scheme for detection of masses in whole breast ultrasound images. Med Phys. 2007;34:4378–88.
18. Cheng HD, Shan J, Ju W, Guo Y, Zhang L. Automated breast cancer detection and classification using ultrasound images: a survey. Pattern recognit. 2010;43:299–317.
19. Nie K, Chen JH, Chan S, Chau MK, Yu HJ, Bahri S, Tseng T, Nalcioglu O, Su MY. Development of a quantitative method for analysis of breast density based on three-dimensional breast MRI. Med Phys. 2008;35:5253–62.
20. Agner SC, Soman S, Libfeld E, McDonald M, Thomas K, Englander S, Rosen MA, Chin D, Nosher J, Madabhushi A. Textural kinetics: a novel dynamic contrast-enhanced (DCE)-MRI feature for breast lesion classification. J Digit Imaging. 2011;24:446–63.
21. Minoura N, Teramoto A, Takahashi K, Yamamuro O, Nishio M, Tamaki T, Fujita H. Preliminary study on an automated extraction of breast region and automated detection of breast tumors and axillary metastasis using PET/CT images. Med Imaging Technol. 2017;35:158–66.
22. Tanaka E, Kudo H. Optimal relaxation parameters of DRAMA (dynamic RAMLA) aiming at one-pass image reconstruction for 3D-PET. Phys Med Biol. 2010;55:2917–38.
23. Keyes JW. SUV: standard uptake or silly useless value? J Nucl Med. 1995;36:1836–9.
24. Li Q, Sone S, Doi K. Selective enhancement filters for nodules, vessels, and airway walls in two- and three-dimensional CT scans. Med Phys. 2003;30:2040–51.
25. Vranjesevic D, Schiepers C, Silverman DH, Quon A, Villalpando J, Dahlbom M, Phelps ME, Czernin J. Relationship between 18F-FDG uptake and breast density in women with normal breast tissue. J Nucl Med. 2003;44:1238–42.